Toward high-resolution period-dependent seismic monitoring of tropical cyclones

Lise Retailleau[1], Lucia Gualtieri[2]

Lucia Gualtieri, Lise Retailleau; luciag@princeton.edu, retaille@stanford.edu

[1]Stanford University, Department of Geophysics, Stanford, CA 94305, USA.

[2]Princeton University, Department of Geosciences, Guyot Hall, Princeton, NJ 08544, USA.

This article has been accepted for publication and undergone full peer review but has not been through the copyediting, typesetting, pagination and proofreading process, which may lead to differences between this version and the Version of Record. Please cite this article as doi: 10.1029/2018GL080785

Pioneering work in the mid-twentieth century laid the foundation for our understanding of secondary microseism generation by tropical cyclones. Yet, tracking their sources and linking them to the mechanisms that generate these signals remain challenging. Here, we successfully retrieve the seismic sources associated with typhoon Ioke (2006) with an unprecedented 3-hour resolution and in the entire secondary microseism period band ($T = 2 - 9$ s). Our results indicate that the seismic sources follow the tropical cyclone at a constant distance from its center, corresponding to 34-kt winds. We also assess the link between the generation of the long period secondary microseism signals and the increase of the typhoon propagation speed. This accurate location of seismic sources may provide a new dataset for imaging the Earth's interior and allow for new insights on the interaction between the atmosphere, the ocean, and the solid Earth.

Keypoints:

- Secondary microseism sources of a tropical cyclone are observed over its complete life cycle.
- Seismic sources are located at a nearly constant distance from the center of the cyclone, corresponding to 34-kt winds.
- Secondary microseism sources at long period can only be observed when the tropical cyclone moves fast.

1. Introduction

Tropical cyclones (TCs), called typhoons in the northwestern Pacific Ocean, are among the strongest and most destructive natural phenomena on Earth. While moving over the ocean, they perturb the sea state. Ocean gravity waves driven by typhoon winds move in all directions, interact with each other and generate secondary microseisms [*Longuet-Higgins*, 1950, 1953], the ubiquitous seismic background signal of the Earth at periods between about 2 and 9 s. Better understanding of how secondary microseisms are generated by TCs is key for learning how the solid Earth, the ocean and the atmosphere exchange energy. Moreover, seismic data can bring crucial information (such as TC intensity) to constrain our long-term knowledge of these events [*Gualtieri et al.*, 2018], and more generally of our changing climate [e.g. *Grevemeyer et al.*, 2000].

Seismic signals generated by TCs have high amplitudes on seismic records when the event moves across the ocean and on land. TCs making landfall yield to specific features in the seismic records [e.g. a shift in the frequency content, *Ebeling and Stein*, 2011]. Their energy decay on land is also observable from seismic data [e.g. *Tanimoto and Lamontagne*, 2014; *Tanimoto and Valovcin*, 2015]. However, TCs transfer most of their energy to the solid Earth while they move over the ocean from the coupled atmosphere-ocean system. Clear imprints of TCs have been recorded by ocean bottom seismometers [e.g. *Latham et al.*, 1967; *Lin et al.*, 2014; *Davy et al.*, 2014] and land seismic stations [e.g. *Sufri et al.*, 2014; *Gualtieri et al.*, 2018].

The generation mechanism of secondary microseisms by TCs over the ocean is a particular case of ocean wave-wave interaction [*Longuet-Higgins*, 1950; *Ardhuin et al.*, 2011;

Kedar et al., 2008; *Gualtieri et al.*, 2013; *Ardhuin et al.*, 2015], where a moving storm over-runs its previously generated swells. For example, in the northern hemisphere, as a TC moves and TC's winds rotate counter-clockwise, at time t swells move toward the direction of motion on the East side of the TC. At time $t + \Delta t$, they interfere with swells moving toward the opposite direction generated on the West side of the TC. Their interaction is therefore expected to occur in the wake of the TC itself [*Longuet-Higgins*, 1953].

Several recent studies focused on the seismic sources caused by TCs and on the coupling between the ocean and the solid Earth. However, sources of secondary microseisms generated by TCs have only been observed so far in a few specific cases: a) in the absence of other major storms and cyclones, for well-isolated TCs, b) only during a portion of the TC life-cycle, mostly when the events were particularly strong or fast, and c) at narrow-banded seismic periods, mostly around 5 s. Pioneering observations of body wave sources due to tropical storms and cyclones were made by *Haubrich and McCamy* [1969]. Polarization analysis allowed the measurement of the arrival directions of secondary microseisms generated by hurricane Sandy [*Sufri et al.*, 2014], while travel-time measurements of cross-correlated records have been used to locate the corresponding source regions during one hour of peak hurricane activity [*Chen et al.*, 2015]. Furthermore, using classical beamforming techniques and data narrow-filtered around 5 s, sources of secondary microseisms generated by hurricane Katrina have been located during its 24-hour peak activity [*Gerstoft et al.*, 2006], while sources of typhoon Ioke have been located mostly during the late stage activity of the typhoon [*Zhang et al.*, 2010b; *Gualtieri et al.*, 2014; *Farra et al.*, 2016]. *Zhang et al.* [2010a] further investigated sources from typhoon Ioke at $4.7 - 10$ s period, during two days of the late-stage activity of the typhoon.

In this paper we show that, employing a novel method based on the backprojection of multi-phase body wave arrivals [*Rost and Thomas*, 2002; *Retailleau et al.*, 2015, 2017], we can locate sources of TCs during their entire life cycle and over the entire secondary microseism period band ($T = 2 - 9$ s). Before extending this method over TCs in different ocean basins and over several TC peak seasons, here we present the case study of typhoon Ioke, which occurred in August-September 2006 in the central and northwestern Pacific Ocean. With respect to previous publications [e.g. *Zhang et al.*, 2010b, a; *Gualtieri et al.*, 2014; *Farra et al.*, 2016], we are able to monitor typhoon Ioke during its entire life cycle with higher time and space resolutions, and over a wider period band. This allows us to link the generation of the seismic sources to its propagation characteristics.

In section 2, we describe the method and the data used in this study. We also show the location of the sources of secondary microseisms over time compared to the trajectory of the typhoon and the consequent reconstruction of the entire typhoon track through seismic sources. In section 3, we analyze the location of the sources over both time and frequency in the entire secondary microseism period band ($T = 2 - 9$ s) and compare them to the typhoon track. We infer the relationship between the location of seismic sources and both strength and direction of the typhoon, and we discuss the generation of long-period secondary microseisms as a function of the typhoon speed and the group velocity of ocean gravity waves. We conclude our manuscript with section 4, where we set this work against the context of future studies.

2. Tracking typhoon Ioke

Beamforming and backprojection of seismic waveforms recorded by an array of seismic stations are classical techniques for locating seismic sources [e.g. *Rhie and Romanowicz*, 2004; *Ishii et al.*, 2005]. Beamforming techniques must be adapted to locate sources of secondary microseisms and capture their variability in frequency, time and space. Assessing the sources of secondary microseisms is a way to track these events, and better understand the underlying seismic generation mechanisms. In this section, we show how we can track typhoon Ioke by using secondary microseisms and a novel backprojection technique.

The track, intensity and size of typhoon Ioke are recorded every 6 hours from satellites. The intensity of a TC is defined as the 1-min mean sustained surface wind speed and the size of a TC as the radius that incorporates wind speeds larger than a given threshold. We use center locations and intensities of typhoon Ioke from the Joint Typhoon Warning Center (JTWC) best-track dataset [*Chu et al.*, 2002, `http://www.usno.navy.mil/NOOC/nmfc-ph/RSS/jtwc/best_tracks/`]. Two TC datasets are used to identify its size at two different thresholds: the JTWC best-track dataset with a threshold at 34-kt (1 kt = 0.514 m/s) winds, and a dataset built using storm-centered infrared imagery [*Knaff et al.*, 2014, 2015] with a threshold at 5-kt winds.

The inset on the top right corner of Figure 1 shows the track of typhoon Ioke as a function of time. The white mark along the track in the inset denotes the main turning point of its life cycle – the transition from a tropical storm to a TC. Ioke was an extremely powerful and long-lived typhoon that formed in the Central Pacific Ocean as a tropical depression on August 17, 2006. The cyclone was classified as a typhoon (sustained wind speed > 33 m/s) on August 21, 2006, and while moving west-northwestward it reached the Category-5 intensity on the Saffir-Simpson scale (sustained wind speed > 70 m/s) multiple times. Ioke weakened to a tropical storm while moving east of Japan, just after performing the tropical-extratropical transition (i.e. moving into the midlatitudes, north of $30° - 40°$ N), and it was declared as an extra-tropical storm on September 6 by the JTWC. The storm lost its tropical characteristics assuming an asymmetric shape, but the extra-tropical remnants of Ioke were documented later on with strong winds in the Gulf of Alaska.

In order to locate the seismic sources, we use available seismic data recorded by the vertical component of 230 stations located in central California (black dots in the inset in Figure 1) from August 17, 2006, to September 8, 2006. The seismic waveforms are downloaded from the Incorporated Research Institutions for Seismology (IRIS, http://www.iris.edu/mda), the Northern California Earthquake Data Center [*NCEDC*, 2014] and the Southern California Earthquake Data Center [*SCEDC*, 2013] by using the python toolbox *obspy* [*Krischer et al.*, 2015]. The instrumental response is deconvolved from the raw short-period (119 EH-channel and 27 SH-channel) seismograms, and broadband (78 BH-channel and 4 HH-channel) seismograms in order to get ground velocity. Seismograms are downsampled to 2 Hz and filtered using a Butterworth bandpass filter in three narrow period bands: $2 - 4$ s, $4 - 6$ s and $6 - 9$ s.

The method used in this study to back-project seismic waveforms has been described and widely tested by *Retailleau et al.* [2015, 2017]. It consists in targeting the energy of selected body-wave phases using their slowness, which is directly linked to the distance between the source and the receiver. Body-wave phases are more localized in space and time than surface waves, and therefore their arrival gives more precise information about the location of the sources. As a consequence, our method allows us to locate the sources with high precision using only one array, as demonstrated with earthquake sources by *Retailleau et al.* [2015].

We select the energy that corresponds to the targeted phase in the time-slowness domain from Vespagram analyses performed on a grid of potential locations. Classical techniques for performing array analysis [e.g. *Haubrich and McCamy*, 1969; *Cessaro*, 1994] search for source location by back-projecting the azimuth and slowness extracted from a 2D wavenumber diagram obtained by beamforming [*Rost and Thomas*, 2002]. Our method directly searches for the location of the sources, instead of locating the sources by using the azimuth of the incoming waves, leading to a much more precise spatial resolution (see *Retailleau et al.* [2015, 2017] for more details).

To verify the consistency of our results over time, we interpolate the typhoon track every 3 hours to define the center of the grid ($20° \times 20°$ in longitude and latitude, with a grid spacing of 0.5 degrees) of potential locations of the seismic source. For each point of the grid, we compute a Vespagram [*Rost and Thomas*, 2002] (see Figure S1 in the Supplementary Materials), for a 0.334 s$\cdot$deg^{-1} slowness range centered around the P-wave theoretical slowness predicted in the 1D Earth model IASP91 [*Kennett and Engdahl*, 1991] at a distance corresponding to the one between the network and the potential location [*Crotwell et al.*, 1999; *Krischer et al.*, 2015]. We extract the median value over time and the mean value over the slowness. This selection allows us to remove automatically any other signals having a short duration, like earthquakes and instrumental glitches. Because very strong earthquakes could still bias our results, we remove any signals having standard deviation larger than 15 times the mean over a window of 4 hours.

We apply this method every 3 hours during the entire life cycle of the event, while Ioke was a tropical depression/storm (August 17-20), a TC (August 21-September 6) and an extratropical storm (after September 6). As discussed previously, Ioke lost the tropical characteristics on September 6 and became an extratropical storm, whose centroid location is no longer available from databases due to its asymmetric shape. Therefore, in order to detect additional late signals generated when Ioke was no longer active as a TC, we extrapolate a potential track toward Alaska between September 6 and September 8 (dark magenta in Figure 1) to determine the center of the grid search.

The main panel in Figure 1 shows the typhoon-track location (magenta dots) compared to the seismic sources at $4-6$ s. The larger colored dots represent the location of the maximum amplitude of the backprojection at each time step, corresponding to the most likely location of the seismic sources over time. The three gray-scale snapshots are examples of the normalized beam power resulting from the backprojection analysis, corresponding to August 17, September 1, and September 7; upward triangles represent the location of the typhoon along the track at these times. Downward triangles mark the location of the maximum beam power corresponding to the most likely location of the seismic source (see also movie S1).

At the beginning of the storm activity (August 17 to 21), while Ioke was mostly a tropical depression and a tropical storm (wind speed smaller than 33 m/s), the backprojection analysis does not show any clear evidence of seismic sources. The location of the maximum amplitude of the beam power is highly scattered, and it does not appear to be related to the typhoon track (blue dots in Figure 1). The first snapshot of the beam power shown in Figure 1 illustrates this case: the pattern of the beam power is highly disorganized, and the maximum beam power (identified by the downward blue triangle) is clearly not associated with Ioke. During this stage of the event, while Ioke was a tropical depression and storm, it was likely not strong enough to produce a coherent pattern of ocean waves, preventing their interaction, and in turn the generation of seismic sources.

From August 22 to September 5, the backprojection results become more consistent and start following the typhoon track closely. The second snapshot of the beam power shown in Figure 1 and centered at latitude 20°N is an example of a well-detected source. Seismic sources always follow the event, as documented for portions of the Ioke typhoon track by *Zhang et al.* [2010b, a]; *Gualtieri et al.* [2014]; *Farra et al.* [2016] and for other TCs by *Gerstoft et al.* [2006]; *Haubrich and McCamy* [1969]. The location at which the beam power is maximum (denoted by the downward triangle in orange) is behind the event itself (denoted by the upward triangle in magenta). While previous studies by *Zhang et al.* [2010a] and *Farra et al.* [2016] obtained results on daily time windows, in this study we identified sources with a 3-hour resolution. An interesting and novel aspect, as we will see in detail in the next section, is that this high resolution allows us to observe that the distance between the seismic sources and the event over time is nearly constant during the entire typhoon life cycle (see movie S1).

During the last stage of the event (September 6 onward), Ioke was declared an extra-tropical storm, losing its tropical characteristics. For that reason, we are not able to associate a track to this stage of the event. To define the grid for the backprojection, we extrapolate the typhoon track (dark magenta in Figure 1). An example is provided by the third snapshot of the beam power, center at about 60°N. The associated seismic source (whose maximum is denoted by the downward red triangle) is still well visible, and Ioke can be still tracked as an extra-tropical storm. It is interesting to observe that, although the typhoon weakened during this last stage, we can still observe the seismic sources following the event, while this was not the case at the beginning of the event. *Zhang et al.* [2010a] analyzed seismic signals between September 5 and September 7 averaging over 24 hours, but their maximum beam power is spread over a large region and it is difficult to identify the most likely location of the source with respect to the event.

As demonstrated by *Retailleau et al.* [2015, 2017], our method is able to locate seismic sources with high precision. In Figure S2 we show the spatial uncertainty of the source location associated with the slowness range used in this study to isolate the P-wave energy. We observe that the spatial uncertainty is always smaller than the distance between the event and the seismic source, making the analysis of the distance (as shown in Figure 2) robust.

Similar results can be obtained using data filtered at shorter periods, between 2 and 4 s (see Figure S3). On the other hand, as we will see in the next section, secondary microseisms at longer periods, between 6 and 9 s, are only generated by Ioke toward the end of its life cycle (see Figure S4 and the following section).

3. Linking the seismic sources with the characteristics of the typhoon

For a majority of the previous studies, typhoon Ioke was observed seismologically only around 5 s period [e.g. *Farra et al.*, 2016]. *Zhang et al.* [2010a] further analyzed seismic signals on a broader band, between 4.7 and 10 s, but only during 48 hours of the late stage activity of the typhoon, while Ioke weakened. In this study, we searched for seismic sources associated with Ioke in the whole secondary microseism period band, between 2 and 9 s. The sources retrieved filtering the data in three period bands ($2-4$ s, $4-6$ s, $6-9$ s) reveal features that can be linked to some of the main characteristics of the typhoon. In this section, we restrict our analysis to the portion of the event for which we have a precise location given by the JTWC, between August 17, 2006, to September 6, 2006. Thus we exclude the last extra-tropical portion of the event.

In Figure 2a, we first analyze the distance between the center of the typhoon and the seismic sources, defined as the maxima of the beam power as a function of time and seismic period (colored dots). We perform this analysis using the location of seismic sources corresponding to our available satellite data, that is every 6 hours. The background color represents the TC intensity defined by the Saffir-Simpson scale. We observe that seismic sources at periods shorter than 6 s (blue and red dots) behave differently than seismic sources at periods longer than 6 s (gray dots).

In all the three period bands ($2-4$ s, $4-6$ s, $6-9$ s), at the beginning of the event (August 17 - August 22), the maximum beam power is located far away (distance larger than about 15°) from the event. In the previous section, we observed that our seismic detections during this portion of the event were not related to Ioke (Figure 1). This time period mostly corresponds to the time when Ioke was a tropical depression and a tropical storm (light blue background in Figure 2a), that is when it was not yet classified as a typhoon.

At periods shorter than 6 s (red and blue dots in Figure 2), we observe a delay of about 24 hours between the strengthening of the event to a Category-1 typhoon (green background in Figure 2 on August 21) and the appearance of the seismic sources close to it (August 22). This delay between the strengthening of the event and the emergence of the seismic signals associated to it was previously observed at periods 4 to 7 s for several TCs [*Gualtieri et al.*, 2018], and it is likely related to the non-linear coupling between the atmosphere and the ocean, and a potentially slow wind-wave growth which may take from a few hours to a few days [*Hasselmann et al.*, 1973; *Ochi*, 2003]. After August 22, the seismic sources approach the event and get more organized, maintaining a nearly constant distance over time from the center of the typhoon (Figure 2a). The source location most closely tracks the 34-kt wind size during the entire life cycle of the event, corresponding in the case of typhoon Ioke at a distance of about 2° (green dashed line in Figure 2a). We also observe that the major part of the sources at periods smaller than 6 s (blue and red dots in Figure 2a) are located within the threshold of 5-kt winds (dotted green line in Figure 2a).

In the inset on the top-right corner of Figure S2, we show a zoom of the seismic sources and their spatial uncertainty, together with the corresponding satellite locations (red dots) and the 34-kt wind threshold (red circles). Even taking into account the spatial uncertainty, we observe that the 34-kt wind is still a good approximation for locating the sources.

Consistently with past studies [e.g. *Gerstoft et al.*, 2006; *Zhang et al.*, 2010b, a; *Gualtieri et al.*, 2014; *Farra et al.*, 2016; *Gualtieri et al.*, 2018], T=4-6 s is the period band at which the seismic signals due to the typhoon emerge with higher signal-to-noise ratio. The seismic sources are located in the wake of the typhoon, and they follow the typhoon track (Figure 1). As shown in Figure 2b, at periods between 4 and 6 s, the azimuth of the sources with respect to the track (blue dots) is consistent with the azimuth of the track itself (red dots) during the entire life cycle of the event. The azimuth of the track (red dots) shows that the typhoon turned eastward (azimuth larger than 180°) after September 5, 2006, at 6 am. The seismic sources followed this behavior with a delay of about 12 hours (after September 5, 2006, at 6 pm). These turning points are located between 30° and 40° N, corresponding to its tropical-extratropical transition [e.g. *Evans et al.*, 2017].

At periods longer than 6 s (gray dots in Figure 2a), the sources approach the event and their distribution gets more organized only after September 2, 2006 (see also Figure S4). *Zhang et al.* [2010a] analyzed seismic signals at similar seismic periods averaging the beam power over UTC 12h September 5 through September 7. They identified a weak maximum beam power spread over more than 20° both in latitude and in longitude, falling north of Japan and mostly on land. They do not identify any sources in deep water close to the typhoon track, and relate their findings with possible coastal sources. On the other hand, we identify sources following the typhoon at periods between 6 and 9 s during September 2 to September 8.

Haubrich and McCamy [1969] showed that a fast-moving storm, like a TC, has to override its own ocean waves in order to generate seismic sources in the wake of the event. Only when the event is faster than its own generated ocean waves, seismic sources can be formed in the wake of the event. Therefore, a cutoff period must exist when the propagation speed of the typhoon V equals the group velocity of ocean waves U. At periods below the cutoff period, ocean waves move slower than the storm and seismic sources should appear in the wake of the event. The corresponding cutoff period of seismic waves T_c is half the one of ocean waves. Considering that the seismic sources identified in this study are all located in a deep-water environment, the cutoff period of the generated seismic waves can be obtained using the dispersion relation of ocean gravity waves in deep water $U = \frac{1}{2}\sqrt{\frac{g}{k}}$, where g is the gravitational acceleration, and k is the wavenumber of ocean waves. Imposing $U = V$, the cutoff seismic period is

$$T_c = 2\pi \frac{V}{g} \tag{1}$$

Figure 3 shows the seismic cutoff period T_c (black dots) associated with the propagation speed of typhoon Ioke (background color) as a function of time, computed with Equation (1). This equation implies that observing seismic signals at a given period requires that the event move at least at a given minimum speed. Therefore, long-period signals can be observed only when the event moves fast enough. In the case of typhoon Ioke, this corresponds to the final stage of the event, when Ioke moved northward into the midlatitudes and accelerated after the tropical-extratropical transition.

We observe that the theoretical cutoff period (black dots in Figure 3) underestimates the actual observations (Figure 2a) by about 2 s. However, Equation (1) is a simple relationship and it does not take into account other non-linear processes and heterogeneities of the ocean wave field that may be present during the generation of seismic waves by a TC. Therefore, while it only gives an indication of the period band at which the sources are expected, this simple relationship confirms that, while seismic signals due to Ioke at short period ($T \lesssim 6$ s) can be observed for the whole duration of the TC, signals at long period ($T \gtrsim 6$ s) can only be generated at the end of the event.

4. Conclusion

Backprojection of the P-wave arrivals at a seismic network in California shows evidence of the seismic sources following typhoon Ioke during its entire life cycle and in the entire secondary microseism period band ($2-9$ s). We conduct this observation with an unprecedented 3-hour time resolution and reconstruct the typhoon track with high accuracy. We detect seismic sources continuously from about 24 hours after Ioke became a Category 1 typhoon. The sources are located at a nearly constant distance from the typhoon center, corresponding to 34-kt winds. We also show that the generation of the sources at long period ($6-9$ s) is linked, at the first-order approximation, with the propagation speed of the typhoon, as theorized by *Haubrich and McCamy* [1969].

The work presented in this paper opens the way to a wide range of future studies. Our method can be easily extended to the analysis of different seismic phases [e.g. *Retailleau et al.*, 2017] recorded on the three components of seismic arrays to exploit the energy partition at the source through detection of shear waves [e.g. *Nishida and Takagi*, 2016].

The method also allows investigating events in different ocean basins and over different seasons, including data for which we have little *a-priori* information from satellites. Moreover, this global scale analysis could complement current satellite information by giving some quantitative constraints on ocean surface processes, which are still very difficult to measure [*Hwang and Walsh*, 2018; *Ardhuin et al.*, 2018]. Finally, by advancing our understanding of the mechanisms lying behind ocean-generated signals, we can improve the current way of performing correlation-based ambient noise tomography and potentially provide a new database, other than earthquakes, to study the deep Earth's interior [*Stehly et al.*, 2016].

Acknowledgments. The dataset was downloaded and processed using *python* and the seismological community scientific library *obspy* [*Krischer et al.*, 2015]. *Python* and *Matlab* were used to analyze the results and make figures. The facilities of IRIS Data Services, and specifically the IRIS Data Management Center, were used to access to the waveforms, related metadata, and/or derived products used in this study (http://www.iris.edu/mda). The IRIS Data Services are funded through the Seismological Facilities for the Advancement of Geoscience and EarthScope (SAGE) Proposal of the National Science Foundation under Cooperative Agreement EAR-1261681. Waveform data, metadata, or data products for this study were accessed through the Northern California Earthquake Data Center [*NCEDC*, 2014]. The SCEDC and SCSN are funded through U.S. Geological Survey Grant G10AP00091, and the Southern California Earthquake Center, which is funded by NSF Cooperative Agreement EAR-0529922 and USGS Cooperative Agreement 07HQAG0008. We thank B. Tolar and S. Pascale for useful comments that helped us to improve the manuscript. We also wish to acknowledge the editor Jeroen Ritsema, Barbara Romanowicz, and an anonymous reviewer for their constructive and helpful reviews.

References

Ardhuin, F., E. Stutzmann, M. Schimmel, and A. Mangeney, Ocean wave sources of seismic noise, *Journal of Geophysical Research: Oceans*, *116*(C9), 2011.

Ardhuin, F., L. Gualtieri, and E. Stutzmann, How ocean waves rock the earth: Two mechanisms explain microseisms with periods 3 to 300 s, *Geophysical Research Letters*, *42*(3), 765–772, 2015.

Ardhuin, F., et al., Measuring currents, ice drift, and waves from space: the sea surface kinematics multiscale monitoring (skim) concept, *Ocean Science*, *14*(3), 337–354, 2018.

Cessaro, R. K., Sources of primary and secondary microseisms, *Bulletin of the Seismological Society of America*, *84*(1), 142–148, 1994.

Chen, X., D. Tian, and L. Wen, Microseismic sources during Hurricane Sandy, *Journal of Geophysical Research: Solid Earth*, *120*(9), 6386–6403, 2015.

Chu, J.-H., C. R. Sampson, A. S. Levine, and E. Fukada, The joint typhoon warning center tropical cyclone best-tracks, 1945–2000, *Ref. NRL/MR/7540-02*, *16*, 2002.

Crotwell, H. P., T. J. Owens, and J. Ritsema, The TauP Toolkit: Flexible seismic travel-time and ray-path utilities, *Seismological Research Letters*, *70*, 154–160, 1999.

Davy, C., G. Barruol, F. R. Fontaine, K. Sigloch, and E. Stutzmann, Tracking major storms from microseismic and hydroacoustic observations on the seafloor, *Geophysical Research Letters*, *41*(24), 8825–8831, 2014.

Ebeling, C. W., and S. Stein, Seismological identification and characterization of a large hurricane, *Bulletin of the Seismological Society of America*, *101*(1), 399–403, 2011.

Evans, C., et al., The extratropical transition of tropical cyclones. Part I: Cyclone evolution and direct impacts, *Monthly Weather Review*, *145*(11), 4317–4344, 2017.

Farra, V., E. Stutzmann, L. Gualtieri, M. Schimmel, and F. Ardhuin, Ray-theoretical modeling of secondary microseism P waves, *Geophysical Journal International*, *206*(3), 1730–1739, 2016.

Gerstoft, P., M. C. Fehler, and K. G. Sabra, When Katrina hit California, *Geophysical Research Letters*, *33*(17), 2006.

Grevemeyer, I., R. Herber, and H.-H. Essen, Microseismological evidence for a changing wave climate in the northeast Atlantic Ocean, *Nature*, *408*(6810), 349, 2000.

Gualtieri, L., E. Stutzmann, Y. Capdeville, F. Ardhuin, M. Schimmel, A. Mangeney, and A. Morelli, Modelling secondary microseismic noise by normal mode summation, *Geophysical Journal International*, *193*(3), 1732–1745, 2013.

Gualtieri, L., É. Stutzmann, V. Farra, Y. Capdeville, M. Schimmel, F. Ardhuin, and A. Morelli, Modelling the ocean site effect on seismic noise body waves, *Geophysical Journal International*, *197*(2), 1096–1106, 2014.

Gualtieri, L., S. J. Camargo, S. Pascale, F. M. Pons, and G. Ekström, The persistent signature of tropical cyclones in ambient seismic noise, *Earth and Planetary Science Letters*, *484*, 287–294, 2018.

Hasselmann, K., et al., Measurements of wind-wave growth and swell decay during the Joint North Sea Wave Project (JONSWAP), *Ergänzungsheft 8-12*, 1973.

Haubrich, R. A., and K. McCamy, Microseisms: Coastal and pelagic sources, *Reviews of Geophysics*, *7*(3), 539–571, 1969.

Hwang, P. A., and E. J. Walsh, Estimating maximum significant wave height and dominant wave period inside tropical cyclones, *Weather and Forecasting*, (2018), 2018.

Ishii, M., P. M. Shearer, H. Houston, and J. E. Vidale, Extent, duration and speed of the 2004 Sumatra–Andaman earthquake imaged by the Hi-Net array, *Nature*, *435*(7044), 933, 2005.

Kedar, S., M. Longuet-Higgins, F. Webb, N. Graham, R. Clayton, and C. Jones, The origin of deep ocean microseisms in the North Atlantic Ocean, *Proceedings of the Royal Society of London A: Mathematical, Physical and Engineering Sciences*, *464*(2091), 777–793, 2008.

Kennett, B., and E. Engdahl, Traveltimes for global earthquake location and phase identification, *Geophysical Journal International*, *105*(2), 429–465, 1991.

Knaff, J. A., S. P. Longmore, and D. A. Molenar, An objective satellite-based tropical cyclone size climatology, *Journal of Climate*, *27*(1), 455–476, 2014.

Knaff, J. A., S. P. Longmore, and D. A. Molenar, CORRIGENDUM: An Objective Satellite-Based Tropical Cyclone Size Climatology, *Journal of Climate*, *28*(21), 8648–8651, 2015.

Krischer, L., T. Megies, R. Barsch, M. Beyreuther, T. Lecocq, C. Caudron, and J. Wassermann, ObsPy: A bridge for seismology into the scientific Python ecosystem, *Computational Science & Discovery*, *8*(1), 014,003, 2015.

Latham, G. V., R. S. Anderson, and M. Ewing, Pressure variations produced at the ocean bottom by hurricanes, *Journal of Geophysical Research*, *72*(22), 5693–5704, 1967.

Lin, J.-Y., T.-C. Lee, H.-S. Hsieh, Y.-F. Chen, Y.-C. Lin, H.-H. Lee, and Y.-Y. Wen, A study of microseisms induced by typhoon Nanmadol using ocean-bottom seismometers, *Bulletin of the Seismological Society of America*, *104*(5), 2412–2421, 2014.

Longuet-Higgins, A theory of the origin of microseisms, *Phil. Trans. R. Soc. Lond. A*, *243*(857), 1–35, 1950.

Longuet-Higgins, Can sea waves cause microseisms, *Nat. Acad. Sci., Washington Publ*, *306*, 74–86, 1953.

NCEDC, National Seismic Networks of Switzerland; ETH Zurich, doi:10.7932/NCEDC, UC Berkeley Seismological Laboratory. Dataset, 2014.

Nishida, K., and R. Takagi, Teleseismic S wave microseisms, *Science*, *353*(6302), 919–921, 2016.

Ochi, M., *Hurricane generated seas*, vol. 8, Elsevier, 2003.

Retailleau, L., N. Shapiro, J. Guilbert, M. Campillo, and P. Roux, Detecting and locating seismic events with using USArray as a large antenna, *Advances in Geosciences*, *40*, 27–30, 2015.

Retailleau, L., M. Landès, L. Gualtieri, N. M. Shapiro, M. Campillo, P. Roux, and J. Guilbert, Detection and analysis of a transient energy burst with beamforming of multiple teleseismic phases, *Geophysical Journal International*, *212*(1), 14–24, 2017.

Rhie, J., and B. Romanowicz, Excitation of earth's continuous free oscillations by atmosphere–ocean–seafloor coupling, *Nature*, *431*(7008), 552, 2004.

Rost, S., and C. Thomas, Array seismology: Methods and applications, *Reviews of Geophysics*, *40*(3), 1008, doi:10.1029/2000RG000100, 2002.

SCEDC, Southern California Earthquake Center, doi:10.7909/C3WD3xH1, Caltech. Dataset, 2013.

Stehly, L., L. Retailleau, P. Boué, S. Durand, L. Li, and M. Campillo, Core Mantle Boundary Imaging underneath the North Atlantic ocean using teleseismic noise correlations, *AGU Fall Meeting 2016*, *S41A-2762*, 2016.

Sufri, O., K. D. Koper, R. Burlacu, and B. de Foy, Microseisms from superstorm Sandy, *Earth and Planetary Science Letters*, *402*, 324–336, 2014.

Tanimoto, T., and A. Lamontagne, Temporal and spatial evolution of an on-land hurricane observed by seismic data, *Geophysical Research Letters*, *41*(21), 7532–7538, 2014.

Tanimoto, T., and A. Valovcin, Stochastic excitation of seismic waves by a hurricane, *Journal of Geophysical Research: Solid Earth*, *120*(11), 7713–7728, 2015.

Zhang, J., P. Gerstoft, and P. D. Bromirski, Pelagic and coastal sources of P-wave microseisms: Generation under tropical cyclones, *Geophysical Research Letters*, *37*(15), 2010a.

Zhang, J., P. Gerstoft, and P. M. Shearer, Resolving P-wave travel-time anomalies using seismic array observations of oceanic storms, *Earth and Planetary Science Letters*, *292*(3-4), 419–427, 2010b.

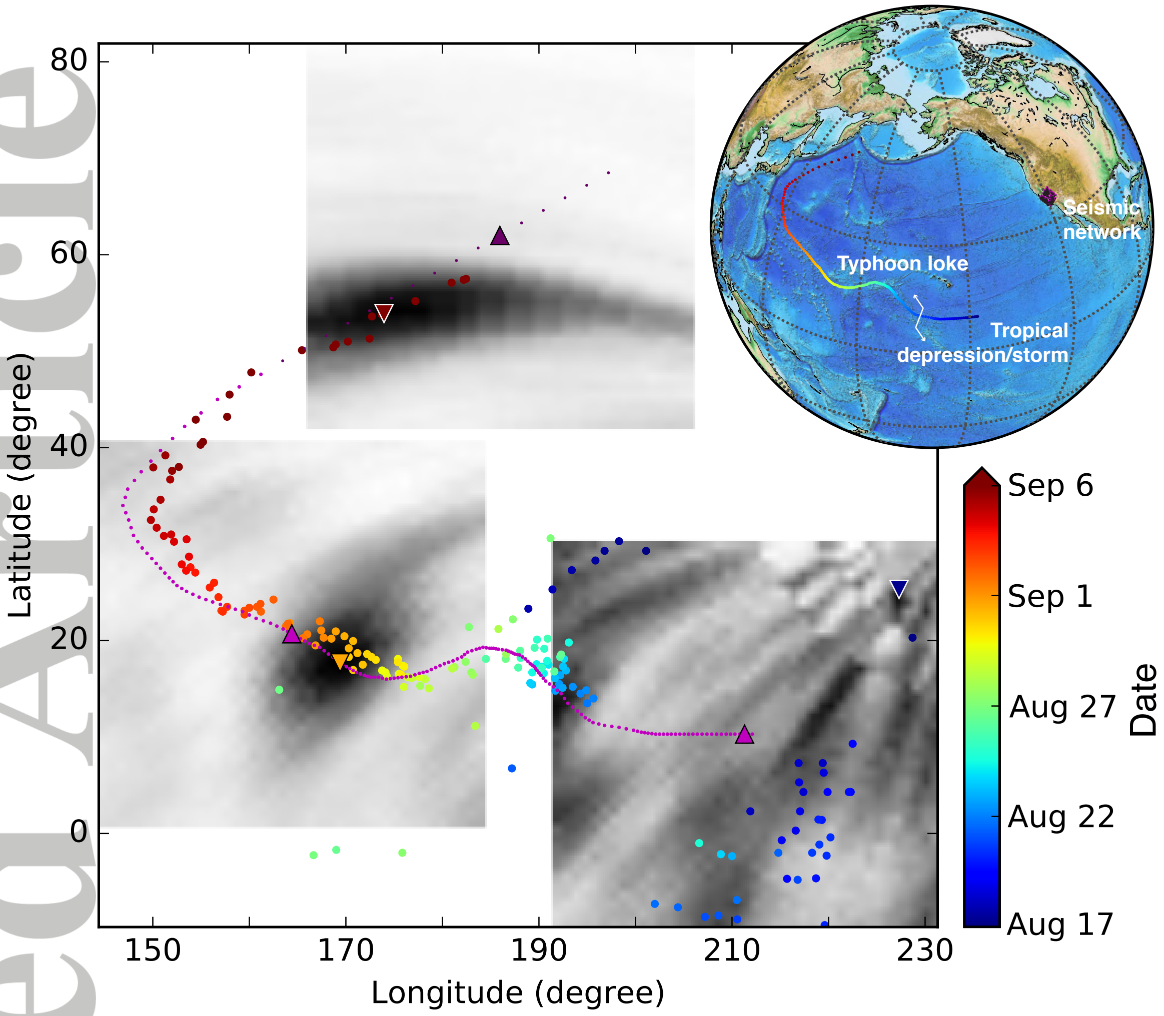

Figure 1. Track of typhoon Ioke from satellite data (magenta small dots) compared to the corresponding seismic sources in the $4-6$ s period band over time (big colored dots). The dots in dark magenta at the end of the track represent the extrapolation of the track when Ioke was an extra-tropical storm. The three gray-scale snapshots show the normalized beam power resulting from the backprojection analysis at three different times. Upward (downward) triangle marks the typhoon location (the seismic source) at these times. The inset on the top-right corner of the figure shows the geographic location of the seismic stations used in this study and the typhoon track (color scale).

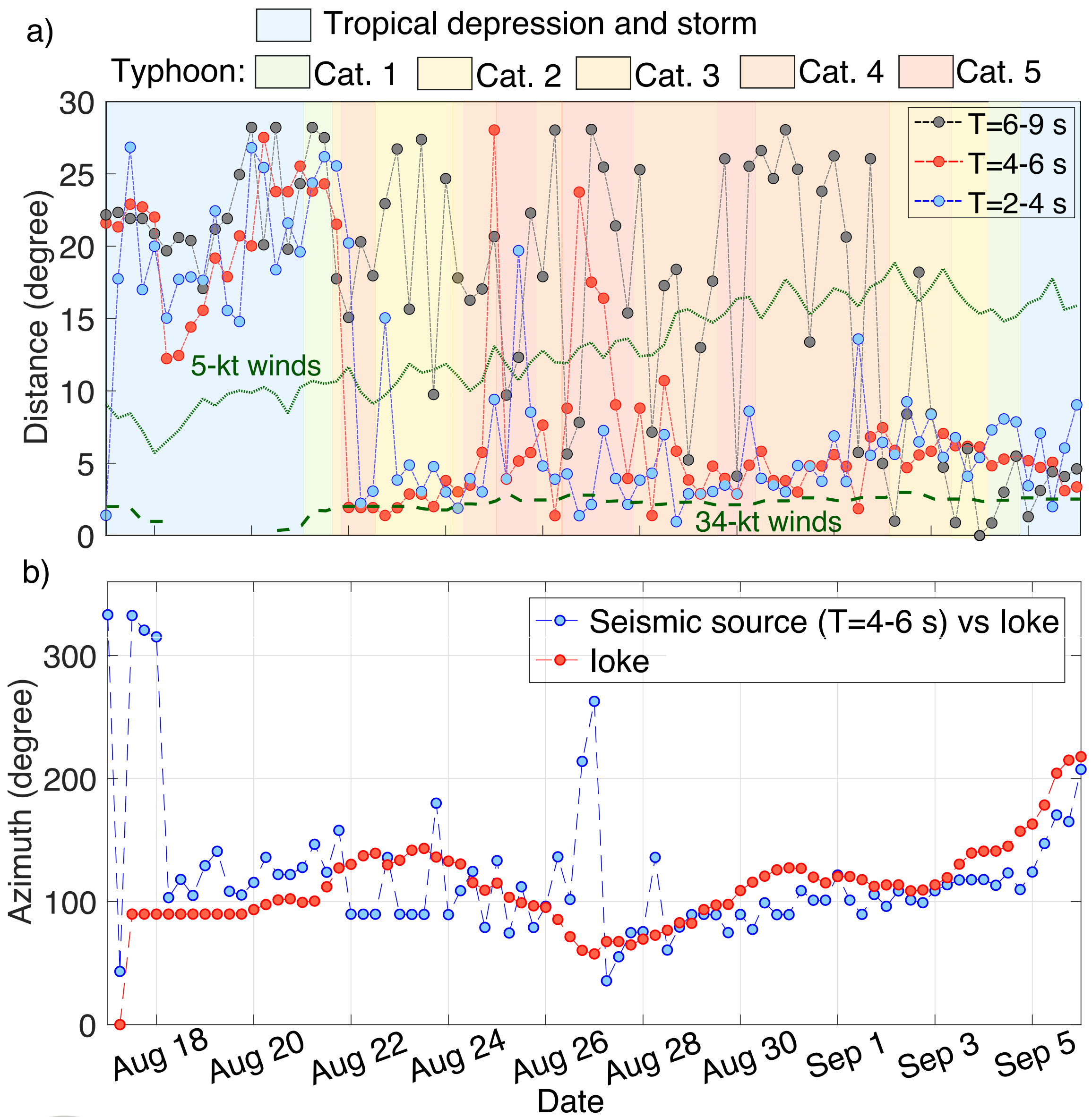

Figure 2. a) Distance between the center of the typhoon and the seismic source as a function of time. Seismic data have been filtered between: $2-4$ s (blue), $4-6$ s (red), and $6-9$ s (gray). The dotted (dashed) green line denotes the typhoon size associated with 5-kt (34-kt) winds. The background color indicates the typhoon intensity through time. b) Azimuth of the typhoon track (red) and of the seismic sources with respect to the typhoon track (blue) as a function of time.

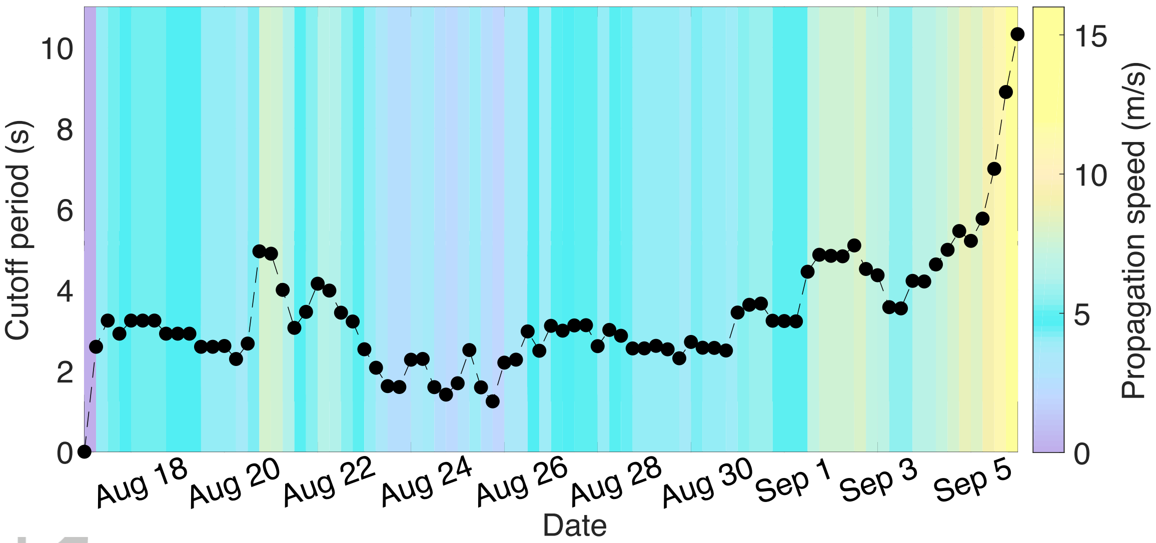

Figure 3. Seismic cutoff period from Equation (1) as a function of time and propagation speed.